ARTICLES
https://doi.org/10.1038/s41566-018-0155-y

nature photonics

Silicon Mie resonators for highly directional light emission from monolayer MoS_2

Ahmet Fatih Cihan[1], Alberto G. Curto[1,2], Søren Raza[1], Pieter G. Kik[1,3] and Mark L. Brongersma[1*]

Controlling light emission from quantum emitters has important applications, ranging from solid-state lighting and displays to nanoscale single-photon sources. Optical antennas have emerged as promising tools to achieve such control right at the location of the emitter, without the need for bulky, external optics. Semiconductor nanoantennas are particularly practical for this purpose because simple geometries such as wires and spheres support multiple, degenerate optical resonances. Here, we start by modifying Mie scattering theory developed for plane wave illumination to describe scattering of dipole emission. We then use this theory and experiments to demonstrate several pathways to achieve control over the directionality, polarization state and spectral emission that rely on a coherent coupling of an emitting dipole to optical resonances of a silicon nanowire. A forward-to-backward ratio of 20 was demonstrated for the electric dipole emission at 680 nm from a monolayer MoS_2 by optically coupling it to a silicon nanowire.

Achieving control over the radiation properties of quantum emitters is key to improving efficiency and realizing new functionality in optoelectronic systems. Bulky optical components have been developed for many years and are extremely effective in controlling the angular, polarization and spectral properties of light emission. Recent advances in the fields of metallic and dielectric optical metamaterials and nanoantennas have now also enabled effective integration of solid-state emitters and control elements into inexpensive platforms[1,2]. Such structures can manipulate light emission in the near field of an emitter and thus promise even greater control over the emission process. For example, we will show how the undesired losses due to radiation of quantum emitters into a high-index substrate can be reduced by redirecting the emission upward with an antenna.

Whereas structures based on noble metals are currently most advanced in manipulating light–matter interaction at the nanoscale, they typically are complex in shape, display undesired optical losses and are not compatible with most semiconductor device processing technologies. High-index semiconductor antennas can circumvent these issues while providing complex electrical and optical functions[3–10]. Based on their mature fabrication infrastructure, silicon nanostructures appear particularly promising for optoelectronic applications[5–8,11–13]. Semiconductor nanoparticles of simple geometric shapes have displayed directional scattering of plane waves when the renowned Kerker conditions are satisfied[8,11,14]. When these conditions are met, directionality is naturally achieved through the coherent excitation of electric and magnetic dipole resonances in the particle and tuning the interference of the associated scattered fields, which was demonstrated in multiple platforms including nanocylinders[8,15–17]. Thanks to their high refractive indices, semiconductor nanoparticles can satisfy the Kerker conditions in the visible spectral range[11,14,18]. Given the ever-increasing importance of solid-state light emitters and quantum nanophotonics, it is of great interest to explore whether analogous conditions can be identified that will facilitate directional emission from quantum emitters, and we answer this important question positively in this work. When the highly localized dielectric resonances are utilized, one can achieve local control over the angular and polarization properties of the radiation pattern without the need for planar or particle-like back reflectors, which makes it versatile and readily applicable in numerous platforms[19,20]. As such, it nicely complements other low-loss approaches involving advanced semiconductor photonic crystals, planar optical antennas and leaky-wave antenna structures to control spectral and angular emission properties[21–28].

Photoluminescence control and directional emission with the help of nanometallic antennas have been analysed theoretically in great detail and demonstrated experimentally at optical frequencies[29–36]. For semiconductor antennas, however, directional emission exploiting Mie resonances has been limited to theoretical proposals[11,37–47] or experiments in the microwave regime[48]. By modifying the conventional Mie theory to describe light scattering by a nanowire from a dipolar source as opposed to the standard plane wave source, we reveal that directional emission with a silicon nanowire can be realized through a variety of mechanisms. Each of these directionality mechanisms involves optical interference effects that come about when the light emitted from a quantum emitter can follow different pathways to the far field. For example, highly directional emission can occur when a fraction of the light emitted by an electric dipole source is rescattered by exciting the dominant electric dipole resonance of a nearby nanowire. It can also follow from the coherent excitation of electric and magnetic dipoles in a nanowire, more akin to the original directional Kerker scattering[40]. Experimental evidence is provided for both of these directionality mechanisms by coupling the exciton emission from an atomically thin layer of MoS_2 (refs [49–52]) to two differently sized silicon nanowires. We demonstrate a forward-to-backward emission ratio of 20 from MoS_2 emitters coupled to silicon nanowires at visible wavelengths. The use of a two-dimensional (2D) semiconductor enables the realization of an accurate and repeatable separation between the emitter and nanowire, which is critical for obtaining reliable control over the direction of light emission[39]. Furthermore, 2D materials such as MoS_2 benefit from the

[1]Geballe Laboratory for Advanced Materials, Stanford University, Stanford, CA, USA. [2]Department of Applied Physics and Institute for Photonic Integration, Eindhoven University of Technology, Eindhoven, the Netherlands. [3]CREOL, The College of Optics and Photonics, University of Central Florida, Orlando, FL, USA. *e-mail: Brongersma@stanford.edu

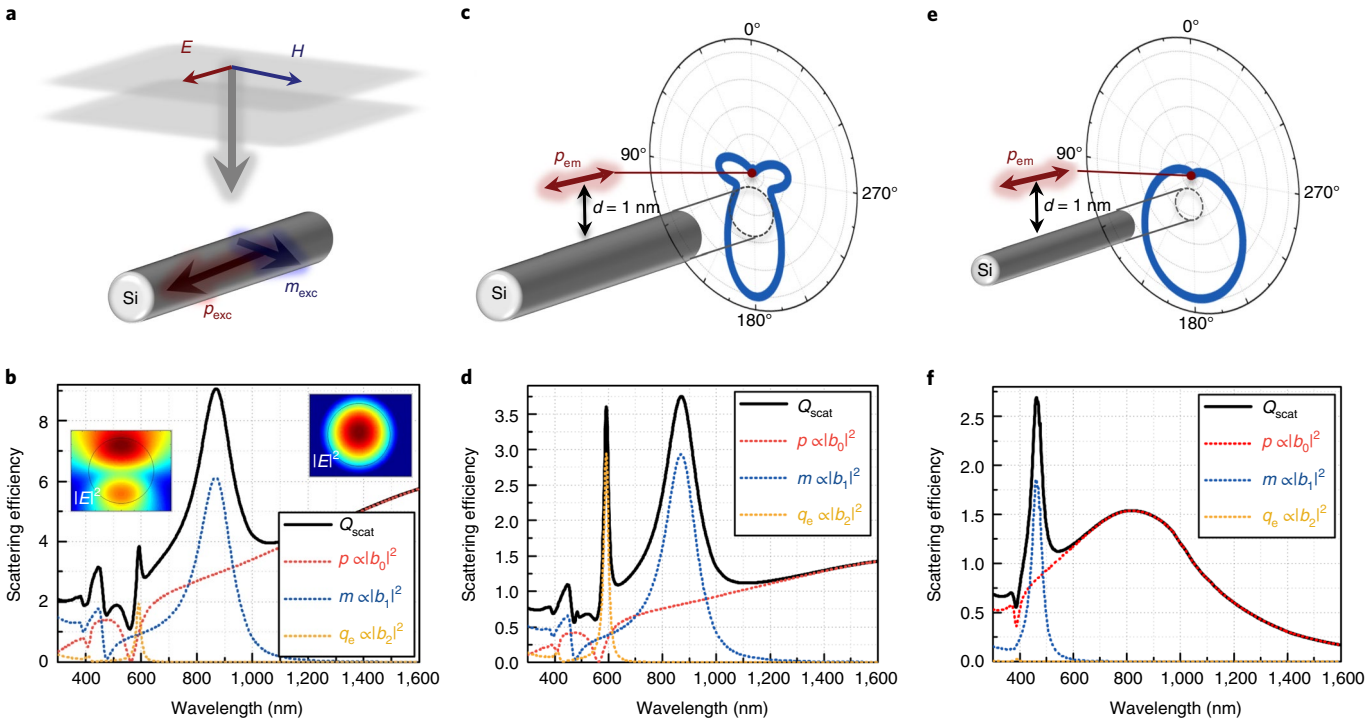

Fig. 1 | Scattering behaviour of a silicon nanowire under plane wave and dipole excitations. a, Schematic of the nanowire under plane wave excitation showing the possible excitation of electric and magnetic dipole resonances (*E* and *H* indicate the electric and magnetic field strength, respectively). **b**, Scattering efficiency and the multipolar contributions from the electric dipole *p*, magnetic dipole *m* and electric quadrupole q_e resonances under plane wave excitation for a nanowire with $R = 88$ nm. Insets are the electric field intensity profiles in the nanowire at the electric (right) and magnetic (left) dipole peak wavelengths. **c**–**f**, Schematic and the radiation pattern for dipole excitation of a nanowire with $R = 88$ nm (**c**) and $R = 38$ nm (**e**) and $d = 1$ nm at $\lambda = 675$ nm (p_{em} denotes the emitter electric dipole). Panels **d**,**f** correspond to the scattering efficiency and its multipolar contributions for cases **c**,**e**, respectively.

simplicity and low-cost nature of available deposition/growth techniques, making them particularly promising for future photonic device applications compared with conventional epitaxially grown emitter materials[53–55].

Modified Mie theory for directional emission

Conventional Mie theory allows us to calculate the excited resonances for an infinitely long cylinder under plane wave illumination (see Fig. 1a for the excitation geometry) by expanding the incident and scattered fields in terms of cylindrical harmonics[56]. The expansion coefficients in the scattered field are referred to as Mie coefficients, and they quantify the scattering contributions from different resonances, for example, electric and magnetic dipoles (see Fig. 1b for a multipolar decomposition of the scattering efficiency Q_{scat} for an infinitely long silicon nanowire). When Mie coefficients corresponding to the electric and magnetic dipoles excited by a plane wave have equal amplitude and phase, the scattered fields originating from these resonances destructively interfere in the backward direction, satisfying the so-called first Kerker condition[15]. This condition has played a central role in the research on light–matter interactions with high-index nanostructures[2]. In this work, we will go beyond plane wave excitation and explore the impact of using the electric dipole emission from the MoS_2 monolayer as our source. We show that the choice of a localized source can profoundly influence the weights of the excited nanowire resonances compared with the plane wave case. This naturally results in different conditions for emission directionality. To gain an intuitive understanding of the origin of these modifications, we derive an analytic expression for the scattering efficiency of a cylindrical nanowire for electric dipole radiation in 2D:

$$Q_{scat}^{dipole} = \frac{P_{scat}}{P_{inc}} = \sum_{n=-\infty}^{\infty} |b_n|^2 |H_n^{(1)}[k_0(R+d)]|^2 \quad (1)$$

Here, P_{scat} and P_{inc} are the scattered and incident source-dipole radiation powers, respectively, b_n are the conventional Mie coefficients found from the plane wave excitation problem[56], $H_n^{(1)}$ are Hankel functions of the first kind, $k_0 = 2\pi/\lambda$ is the free-space wave vector, λ is the wavelength, R is the nanowire radius and d is the dipole–nanowire distance (see Supplementary Information for the derivation of equation (1)). Note that in this 2D analysis, the excitation source is a line dipole and the nanowire is infinitely long[56]. Whereas a three-dimensional (3D) theory would be needed to quantitatively predict the correct magnitude for the scattering efficiency for a point dipole source, we show that this simple 2D description can explain the role of the different multipolar excitations in achieving directional emission and the importance of controlling the nanowire–emitter distance[39]. This is particularly true as, for symmetry reasons, the far-field radiation patterns seen for an infinitesimal electric point dipole (3D) and an electric line source (2D) are identical in the plane orthogonal to the nanowire axis and intersecting the emitter (see Supplementary Fig. 4). Hence, the scattered far-field radiation pattern in this plane will also be identical in both cases[45].

As can be seen in equation (1), each term in the expression for the scattering efficiency can be associated with a specific resonance. More specifically, the terms with b_0 and b_1 Mie coefficients have been associated with electric and magnetic dipole resonances, respectively[43,57]. Each of the resonant contributions has a distance-dependent weighting factor that is given by the Hankel function relevant to that resonance. The origin of this Hankel function

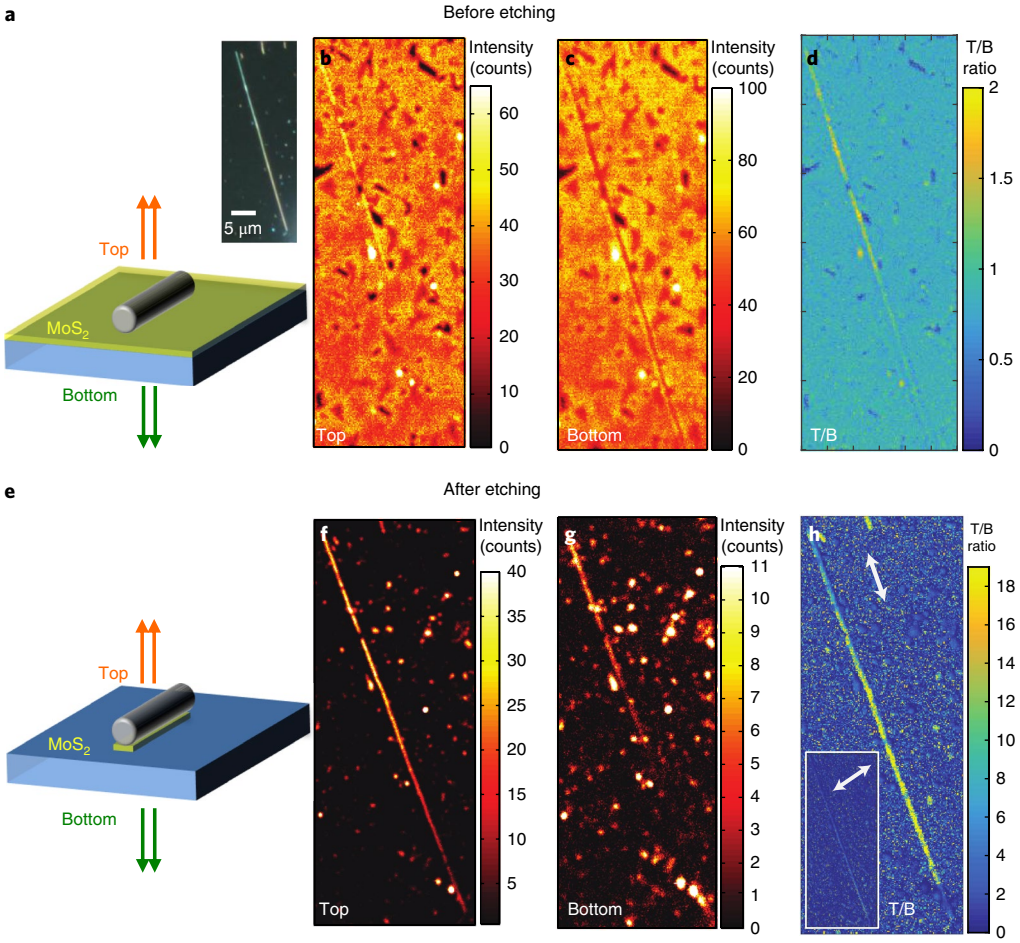

Fig. 2 | Experimental demonstration of highly directional emission in fluorescence images. a, Schematic and dark-field scattering image of an unetched MoS_2 sample. **b**,**c**, Top (T) and bottom (B) fluorescence images of the sample for transverse magnetic polarization. **d**, T/B ratio normalized such that the bare MoS_2 T/B ratio is ~0.8, as predicted by optical simulations for this elementary system (see Methods). **e**–**h**, Corresponding images for the sample after etching the MoS_2 around the nanowire. Inset to **h** shows that the T/B ratio for the transverse electric polarization displays no noticeable enhancement. The arrows indicate the electric field polarization direction for the collected light.

dependence arises as the scattered power is related to the interaction of the dipole source and nanowire scattered fields, which are both described by Hankel functions. Because of these weighting factors, the excitation efficiencies for different multipoles display different dependences on the dipole–nanowire distance, which makes this distance an important parameter determining the directionality of the overall emission. The scattering behaviour of the nanowire under dipole illumination approaches that seen for plane wave illumination when the dipole source is far ($d \gg \lambda$) from the nanowire (Supplementary Fig. 1). However, when the dipole is brought closer to the nanowire as in Fig. 1c, the excitation of different resonances takes place with different strengths, resulting in a modified scattering spectrum (Fig. 1d).

The dipole emission directionality (Fig. 1c) is different from the plane wave scattering directionality not only because of the modified resonance contributions but also because of the non-directional nature of the source[40]. In other words, to achieve the desired emission directionality, it is important to consider the interference of the incident fields from the source and scattered fields from the nanowire as opposed to the plane wave case where typically only the scattered fields are considered[11,14,18].

For a given emitter/emission wavelength, the nanowire radius can be optimized in a thoughtful manner to achieve directional emission; as it controls the nature of the excited resonances, it effectively controls the scattering behaviour. Besides the scattering, the radius also determines the spectral absorption properties of the nanowire. Supplementary Fig. 2 shows that the nanowires of this study display a high scattering efficiency and a low absorption efficiency within the wavelength of interest, justifying the choice of silicon over their plasmonic counterparts. By using nanowires with different radii, one can obtain directionalities with distinct origins even at the same emission wavelength, as seen in Fig. 1c,e. With the larger radius nanowire shown in Fig. 1c, higher-order multipoles can be excited in the emission band of MoS_2 in the range of 650–720 nm, resulting in directionality due to the interference of the scattered fields originating from these multipoles and the emitter dipole. Conversely, with the smaller nanowire of Fig. 1e, we can observe directional emission due to the interference of the scattered fields from the excited electric dipole nanowire resonance with those of the emitter dipole.

Directional emission of MoS_2 using a Si nanowire

To experimentally investigate the emission directionality, we use a confocal optical microscope with a laser excitation wavelength of 633 nm that affords both top and bottom detection of photoluminescence signals (see Methods). As the emitter, we use monolayer MoS_2 grown on a transparent sapphire substrate. Silicon nanowires are drop cast on top, as shown in Fig. 2a. In one experiment, we

use a tapered silicon nanowire whose radius gradually varies from around 20 nm to 40 nm over a length of 40 μm. The gently tapered shape of the nanowire makes it convenient to match the spectrum of the emitter to the different diameter-dependent nanowire resonances that give rise to directionality.

Images of the transverse magnetic polarized emission are taken from the top and bottom of the sample (Fig. 2b,c). They show that the nanowire enhances the emission of the MoS_2 layer to the top (forward direction) while suppressing the emission to the bottom (backward direction). The top-to-bottom (T/B) ratio for the emission, provided in Fig. 2d, reaches 2.5 on the nanowire, while that for bare MoS_2 areas is about 0.8 (see Methods for the procedure to correct for the contribution of the detection system to the measured asymmetry). An important caveat of the measurement in Fig. 2d is that the detection system is diffraction limited, and consequently the region from which photoluminescence is collected is significantly larger than the nanowire diameter. This results in a reduced T/B ratio compared with our simulations due to the contributions from the bare MoS_2 regions adjacent to the nanowire, which produce non-directional emission. To eliminate this unwanted effect and measure the ultimate directionality observable for emitters under the antenna, the sample is etched using a low-energy argon plasma where the nanowire itself acts as an etching mask (see Fig. 2e).

The top and bottom fluorescence images after the etching process show that the emission is almost entirely eliminated from the bare MoS_2 regions, except for isolated spots corresponding to areas of few-layer MoS_2, while the emission from the emitters under the nanowire is maintained (Fig. 2f,g). Note that the bottom emission around the lower half of the nanowire in Fig. 2g is almost completely suppressed, suggesting a very high directionality (see Supplementary Information for top and bottom line scans of the emission across the nanowire). As can be seen in Fig. 2h, the T/B ratio is more than 20 on the part of the tapered nanowire, whereas that of the reference bare MoS_2 is around 0.8. Therefore, it can be concluded that the nanowire directionality enhancement over bare MoS_2 is more than 25-fold.

We provide, as a control experiment, the T/B ratio of the same nanowire for transverse electric polarized collection in the inset of Fig. 2h. Here, the nanowire is barely discernible in the T/B ratio image, implying that the enhanced directionality seen for the transverse magnetic case is linked to multipolar resonances capable of redirecting the emission with this polarization state.

Two mechanisms for directional emission

To explore the nature of the observed directional emission, we use our analytical Mie theory to calculate the T/B emission ratio. Within this approach, the far-field emission intensity is given as

$$I_{\mathrm{ff}}(\theta) = \frac{\omega^2 \mu_0^2 I^2}{8\pi} \left| \sum_{n=-\infty}^{\infty} (-i)^n \{ J_n[k_0(R+d)] - b_n H_n^{(1)}[k_0(R+d)] \} \mathrm{e}^{-in\theta} \right|^2 \quad (2)$$

where J_n is the Bessel function of the first kind, I is the current of the line source, ω is the radial frequency, μ_0 is the magnetic permeability of vacuum, i is the imaginary unit, θ is the emission angle (see Supplementary Information for the derivation). By integrating the far-field intensity values in equation (2) around the forward ($\theta = \pi$) and backward ($\theta = 0$) directions, we obtain the spectral and nanowire size dependence of the T/B emission ratio (see Methods). Figure 3a shows a map of these calculations, revealing multiple clear bands with high T/B ratios. Each band can be identified with a unique directionality mechanism involving different multipolar resonances. Very similar results are obtained with finite-difference time-domain (FDTD) simulations that include the presence of the substrate, as shown in Supplementary Fig. 6a.

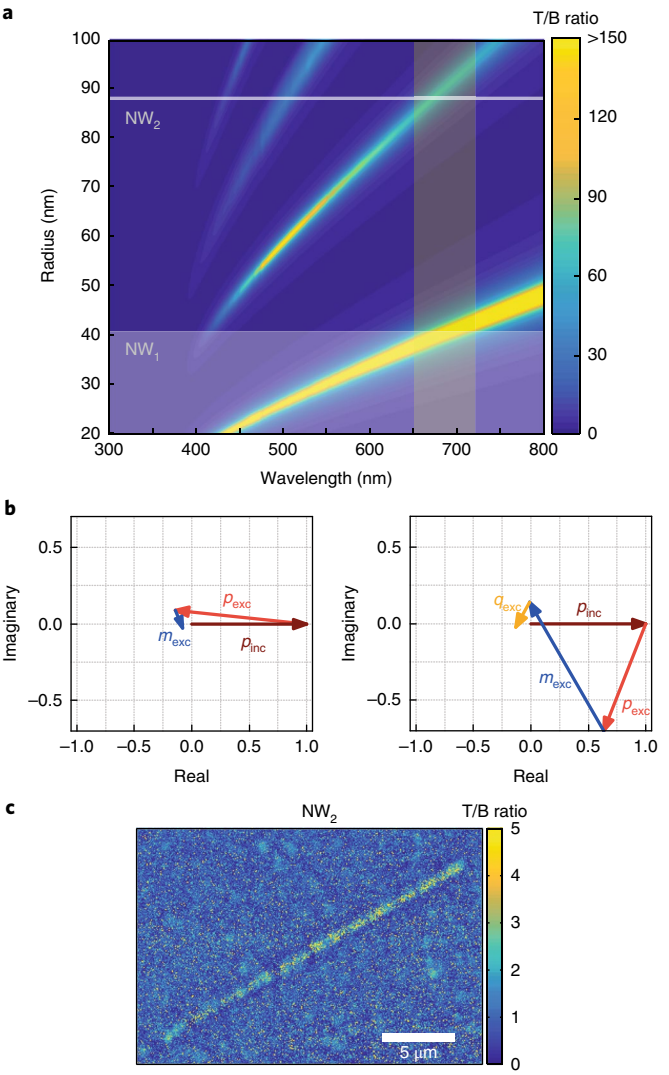

Fig. 3 | Analysis of directionality mechanisms and experimental demonstration of the second mechanism. **a**, T/B ratio of emission of a dipole–nanowire pair obtained with the modified Mie theory (see Methods). The vertical shaded area corresponds to the emission band of MoS_2, and the horizontal shaded band and line indicate the sizes of the two nanowires, NW_1 and NW_2, used in this study. **b**, Phasor representations of the electric fields at a position in the backward emission direction and broken down into different multipolar contributions for nanowires with radii of 38 nm (NW_1, left panel, $\lambda = 660$ nm) and 88 nm (NW_2, right panel, $\lambda = 675$ nm). Labels indicate the sources of each contribution. The electric field due to the source dipole is taken to be 1, and the other components are normalized accordingly. **c**, Map of the experimental T/B ratio for the 88 nm-radius nanowire, obtained in the same way as in Fig. 2.

For the emission wavelength range of MoS_2 (the vertical shaded area in Fig. 3a), it is possible to capture two directionality mechanisms with nanowires that feature radii under 100 nm. To identify how the different multipoles contribute to each mechanism, we determine the far-field complex electric field contributions in the backward direction from several multipolar resonances. We first analyse the smaller, tapered nanowire for which the high directionality was verified in Fig. 2. Its radius range of 20–40 nm is indicated in Fig. 3a by the lower grey shaded band. For a selected 38 nm-radius nanowire, these relevant field contributions are shown in the

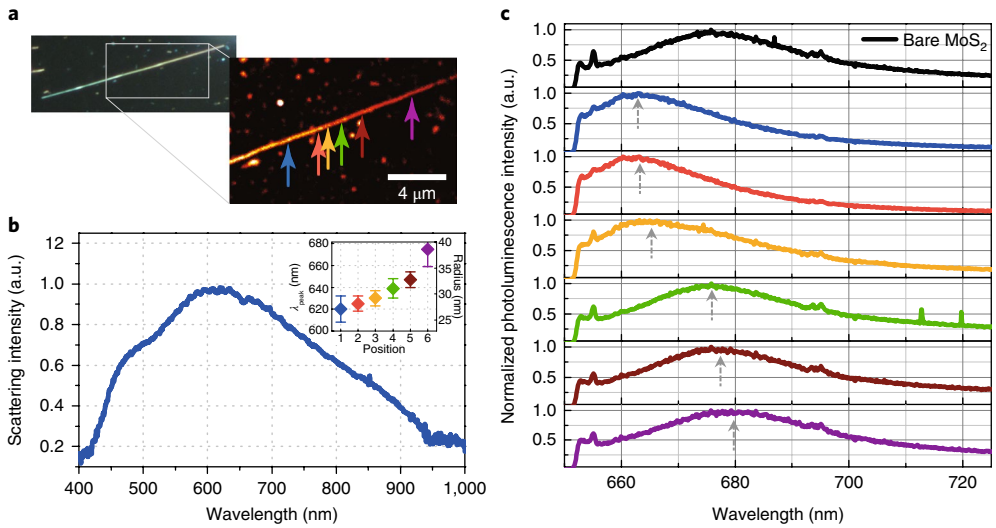

Fig. 4 | Spectral control over the emission wavelength with nanowire size. a, Dark-field scattering image and corresponding zoom-in of the top fluorescence image of the Si nanowire that is tapered from 20 nm (left side) to 40 nm (right side). The coloured arrows indicate the spatial locations along the nanowire where the dark-field white-light scattering and photoluminescence emission spectra are taken. **b**, Dark-field scattering spectrum of the nanowire for transverse magnetic mode collected confocally from the spot on the nanowire corresponding to the blue arrow in **a**. Inset shows the evolution of the scattering peak (λ_{peak}) and the radius obtained by atomic force microscopy as the collection point is moved from left to right on the nanowire. The colours of the data points match the colours of the lines in **a** and **c** (a.u., arbitrary units). **c**, Emission spectra of the system across the nanowire. Each coloured curve corresponds to a position indicated with the same-colour line in **a**. The top black curve is the reference MoS_2 emission spectrum taken from a bare MoS_2 region on the sample. Grey arrows are guides to the eye to visualize the shift in the photoluminescence peak emission wavelength.

left panel of Fig. 3b in a phasor representation to clearly show their relative magnitudes and phases. It is clear that for this wire, the excitation of an electric dipole resonance (p_{exc}) alone suffices to almost fully cancel out the incident field originating from the source dipole in the backward direction. There is only a very small contribution related to the magnetic dipole, m_{exc}. However, for a larger 88 nm-radius nanowire (right panel of Fig. 3b), fields from the electric dipole, magnetic dipole and electric quadrupole resonances (p_{exc}, m_{exc} and q_{exc}, respectively) are more or less equal in magnitude. This results in very little backward emission, and in this case, we find that the directionality can primarily be attributed to the coherent excitation of electric and magnetic dipole resonances. The excitation of these resonances results in scattered fields that cancel the field originating from the source dipole (p_{inc}) in the backward direction. Figure 3c shows experimental evidence of this directionality mechanism. For this 88 nm-radius wire, a T/B ratio in excess of 5 is reached. The lower T/B ratio observed for this larger wire is consistent with the theoretical analysis shown in Fig. 3a.

As with any antenna, the scattered field can produce a back action on the dipole source and an associated Purcell enhancement[58]. As the relative strengths of the source and scattered fields control the directionality, it is important to be aware of such effects. Because our model is an exact solution to Maxwell's equations, the impact of possible Purcell enhancements due to the presence of the nanowire is naturally accounted for.

Spectral control over light emission

Besides the demonstrated angular and polarization control, it is also highly desirable to achieve spectral control over the emission right at the source. This can be attained through a simple variation in the nanowire size[7,59]. For example, Fig. 3a suggests that for each directionality mechanism, the maximum in the T/B ratio will redshift with increasing nanowire size. This is understandable as all of the nanowire resonances that may be involved in achieving directionality redshift with increasing size. At wavelengths where the T/B ratio is large, it is expected that a relatively large fraction of the MoS_2 photoluminescence can be collected in the top direction. It is thus also expected that the photoluminescence spectra collected from the top will redshift as the nanowire size increases. To investigate this point, we analyse a zoomed-in top photoluminescence emission map (see Fig. 4a) from the tapered nanowire that was discussed in Fig. 2. Reflection-mode dark-field white-light scattering spectra taken from different locations along the length of the nanowire show a clear redshift over about 60 nm as the radius increases from 26 nm to 38 nm (see Fig. 4b inset). This comes with a concomitant redshift in the photoluminescence spectrum, as shown in Fig. 4c. As the detection spot is moved along the nanowire length, the emission spectrum is first higher on the blue side of the reference bare MoS_2 emission peak, and ultimately the peak is on the red side of this spectrum (Fig. 4c).

Conclusions

We have experimentally demonstrated directional and spectral control over the visible emission from monolayer MoS_2 emitters with silicon nanowires. A more than 25-fold T/B emission ratio enhancement was observed, indicating that dielectric antennas can be very effective in reducing the undesired emission from quantum emitters into high-index substrates. Conventional Mie theory was extended to the use of an electric dipole source to explain the observed directionality in terms of multipolar contributions with an intuitive analytical model. The insights from this work may find use in realizing high-performance single-photon sources or metasurfaces composed of dense arrays of high-index semiconductor nanostructures to enhance and control light extraction from solid-state light emitters.

Methods

Methods, including statements of data availability and any associated accession codes and references, are available at https://doi.org/10.1038/s41566-018-0155-y.

Received: 30 August 2017; Accepted: 14 March 2018;
Published online: 23 April 2018

References

1. Novotny, L. & van Hulst, N. Antennas for light. *Nat. Photon.* **5**, 83–90 (2011).
2. Kuznetsov, A. I., Miroshnichenko, A. E., Brongersma, M. L., Kivshar, Y. S. & Lukyanchuk, B. Optically resonant dielectric nanostructures. *Science* **354**, aag2472 (2016).
3. Schuller, J., Zia, R., Taubner, T. & Brongersma, M. L. Dielectric metamaterials based on electric and magnetic resonances of silicon carbide particles. *Phys. Rev. Lett.* **99**, 107401 (2007).
4. Cao, L. et al. Engineering light absorption in semiconductor nanowire devices. *Nat. Mater.* **8**, 643–647 (2009).
5. van de Groep, J. & Polman, A. Designing dielectric resonators on substrates: combining magnetic and electric resonances. *Opt. Express* **21**, 1253–1257 (2013).
6. Spinelli, P., Verschuuren, M. A. & Polman, A. Broadband omnidirectional antireflection coating based on subwavelength surface Mie resonators. *Nat. Commun.* **3**, 692 (2012).
7. Staude, I. et al. Shaping photoluminescence spectra with magnetoelectric resonances in all-dielectric nanoparticles. *ACS Photon.* **2**, 172–177 (2015).
8. Paniagua-Domínguez, R. et al. Generalized Brewster effect in dielectric metasurfaces. *Nat. Commun.* **7**, 10362 (2016).
9. Grzela, G. et al. Nanowire antenna emission. *Nano Lett.* **12**, 5481–5486 (2012).
10. Paniagua-Domínguez, R., Grzela, G., Rivas, J. G. & Sánchez-Gil, J. A. Enhanced and directional emission of semiconductor nanowires tailored through leaky/guided modes. *Nanoscale* **5**, 10582–10590 (2013).
11. Staude, I. et al. Tailoring directional scattering through magnetic and electric resonances in subwavelength silicon nanodisks. *ACS Nano* **7**, 7824–7832 (2013).
12. Sautter, J. et al. Active tuning of all-dielectric metasurfaces. *ACS Nano* **9**, 4308–4315 (2015).
13. Cao, L. et al. Semiconductor nanowire optical antenna solar absorbers. *Nano Lett.* **10**, 439–445 (2010).
14. Person, S. et al. Demonstration of zero optical backscattering from single nanoparticles. *Nano Lett.* **13**, 1806–1809 (2013).
15. Kerker, M., Wang, D. & Giles, C. L. Electromagnetic scattering by magnetic spheres. *J. Opt. Soc. Am.* **73**, 765–767 (1983).
16. Geffrin, J. M. et al. Magnetic and electric coherence in forward- and back-scattered electromagnetic waves by a single dielectric subwavelength sphere. *Nat. Commun.* **3**, 1171 (2012).
17. Wiecha, P. R. et al. Strongly directional scattering from dielectric nanowires. *ACS Photon.* **4**, 2036–2046 (2017).
18. Fu, Y. H., Kuznetsov, A. I., Miroshnichenko, A. E., Yu, Y. F. & Luk'yanchuk, B. Directional visible light scattering by silicon nanoparticles. *Nat. Commun.* **4**, 1527 (2013).
19. Atakaramians, S. et al. Strong magnetic response of optical nanofibers. *ACS Photon.* **3**, 972–978 (2016).
20. Ma, X. et al. Solitary oxygen dopant emission from carbon. *ACS Nano* **11**, 6431–6439 (2017).
21. Wierer, J. J., David, A. & Megens, M. M. iii-nitride photonic-crystal light-emitting diodes with high extraction efficiency. *Nat. Photon.* **3**, 163–169 (2009).
22. Noda, S., Fujita, M. & Asano, T. Spontaneous-emission control by photonic crystals and nanocavities. *Nat. Photon.* **1**, 449–458 (2007).
23. Fontana, Y., Grzela, G., Bakkers, E. P. A. M. & Rivas, J. G. Mapping the directional emission of quasi-two-dimensional photonic crystals of semiconductor nanowires using Fourier microscopy. *Phys. Rev. B* **86**, 245303 (2012).
24. Kaniber, M. et al. Highly efficient single-photon emission from single quantum dots within a two-dimensional photonic band-gap. *Phys. Rev. B* **77**, 073312 (2008).
25. Peter, M. et al. Directional emission from dielectric leaky-wave nanoantennas. *Nano Lett.* **17**, 4178–4183 (2017).
26. Chen, H. et al. Enhanced directional emission from monolayer WSe2 integrated onto a multi-resonant silicon-based photonic structure. *ACS Photon.* **4**, 3031–3038 (2017).
27. Chu, X.-L. et al. Experimental realization of an optical antenna designed for collecting 99% of photons from a quantum emitter. *Optica* **1**, 203–208 (2014).
28. Checcucci, S. et al. Beaming light from a quantum emitter with a planar optical antenna. *Light Sci. Appl.* **6**, e16245 (2017).
29. Tong, L., Pakizeh, T., Feuz, L. & Dmitriev, A. Highly directional bottom-up 3D nanoantenna for visible light. *Sci. Rep.* **3**, 2311 (2013).
30. Shegai, T. et al. Unidirectional broadband light emission from supported plasmonic nanowires. *Nano Lett.* **11**, 706–711 (2011).
31. Palacios, E., Park, S., Lauhon, L. & Aydin, K. Identifying excitation and emission rate contributions to plasmon-enhanced photoluminescence from monolayer MoS_2 using a tapered gold nanoantenna. *ACS Photon.* **4**, 1602–1606 (2017).
32. Curto, A. G. et al. Unidirectional emission of a quantum dot coupled to a nanoantenna. *Science* **329**, 930–933 (2010).
33. Curto, A. G. et al. Multipolar radiation of quantum emitters with nanowire optical antennas. *Nat. Commun.* **4**, 1750 (2013).
34. Hancu, I. M., Curto, A. G., Castro-López, M., Kuttge, M. & Van Hulst, N. F. Multipolar interference for directed light emission. *Nano Lett.* **14**, 166–171 (2014).
35. Liu, W., Miroshnichenko, A. E., Neshev, D. N. & Kivshar, Y. S. Broadband unidirectional scattering by magneto-electric core–shell nanoparticles. *ACS Nano* **6**, 5489–5497 (2012).
36. Coenen, T., Bernal Arango, F., Femius Koenderink, A. & Polman, A. Directional emission from a single plasmonic scatterer. *Nat. Commun.* **5**, 3250 (2014).
37. Tian, J., Li, Q., Yang, Y. & Qiu, M. Tailoring unidirectional angular radiation through multipolar interference in a single-element subwavelength all-dielectric stair-like nanoantenna. *Nanoscale* **8**, 4047–4053 (2016).
38. Sikdar, D., Cheng, W. & Premaratne, M. Optically resonant magneto-electric cubic nanoantennas for ultra-directional light scattering. *J. Appl. Phys.* **117**, 83101 (2015).
39. Rolly, B., Stout, B., Bidault, S. & Bonod, N. Crucial role of the emitter–particle distance on the directivity of optical antennas. *Opt. Lett.* **36**, 3368–3370 (2011).
40. Rolly, B., Stout, B. & Bonod, N. Boosting the directivity of optical antennas with magnetic and electric dipolar resonant particles. *Opt. Express* **20**, 1473–1478 (2012).
41. Filonov, D. S. et al. Experimental verification of the concept of all-dielectric nanoantennas. *Appl. Phys. Lett.* **100**, 201113 (2012).
42. Campione, S., Basilio, L. I., Warne, L. K. & Sinclair, M. B. Tailoring dielectric resonator geometries for directional scattering and Huygens' metasurfaces. *Opt. Express* **23**, 2293–2307 (2015).
43. Vynck, K. et al. All-dielectric rod-type metamaterials at optical frequencies. *Phys. Rev. Lett.* **102**, 133901 (2009).
44. Krasnok, A. E., Miroshnichenko, A. E., Belov, P. A. & Kivshar, Y. S. All-dielectric optical nanoantennas. *Opt. Express* **20**, 20599–20604 (2012).
45. Huang, K. C. Y., Jun, Y. C., Seo, M. & Brongersma, M. L. Power flow from a dipole emitter near an optical antenna. *Opt. Express* **19**, 19084–19092 (2011).
46. Albella, P., Shibanuma, T. & Maier, S. A. Switchable directional scattering of electromagnetic radiation with subwavelength asymmetric silicon dimers. *Sci. Rep.* **5**, 18322 (2015).
47. Krasnok, A. E., Simovski, C. R., Belov, P. A. & Kivshar, Y. S. Superdirective dielectric nanoantennas. *Nanoscale* **6**, 7354–7361 (2014).
48. Rolly, B., Geffrin, J.-M., Abdeddaim, R., Stout, B. & Bonod, N. Controllable emission of a dipolar source coupled with a magneto-dielectric resonant subwavelength scatterer. *Sci. Rep.* **3**, 3063 (2013).
49. Mak, K. F., Lee, C., Hone, J., Shan, J. & Heinz, T. F. Atomically thin MoS_2: a new direct-gap semiconductor. *Phys. Rev. Lett.* **105**, 136805 (2010).
50. Wu, S. et al. Monolayer semiconductor nanocavity lasers with ultralow thresholds. *Nature* **520**, 69–72 (2015).
51. Akhavan, S., Cihan, A. F., Bozok, B. & Demir, H. V. Nanocrystal skins with exciton funneling for photosensing. *Small* **10**, 2470–2475 (2014).
52. Splendiani, A. et al. Emerging photoluminescence in monolayer MoS_2. *Nano Lett.* **10**, 1271–1275 (2010).
53. Coleman, J. N. et al. Two-dimensional nanosheets produced by liquid exfoliation of layered materials. *Science* **331**, 568–571 (2011).
54. Xia, F., Wang, H., Xiao, D., Dubey, M. & Ramasubramaniam, A. Two-dimensional material nanophotonics. *Nat. Photon.* **8**, 899–907 (2014).
55. Mak, K. F. & Shan, J. Photonics and optoelectronics of 2D semiconductor transition metal dichalcogenides. *Nat. Photon.* **10**, 216–226 (2016).
56. Bohren, C. F. & Huffman, D. R. *Absorption and Scattering of Light by Small Particles* (Wiley, Weinheim, 1983).
57. Liu, W. et al. Scattering of core-shell nanowires with the interference of electric and magnetic resonances. *Opt. Lett.* **38**, 2621–2624 (2013).
58. Bharadwaj, P., Deutsch, B. & Novotny, L. Optical antennas. *Adv. Opt. Photon.* **1**, 438–483 (2009).
59. Ringler, M. et al. Shaping emission spectra of fluorescent molecules with single plasmonic nanoresonators. *Phys. Rev. Lett.* **100**, 203002 (2008).

Acknowledgements

This research was conducted with the support of the Air Force Office of Scientific Research (AFOSR), Quantum Metaphotonics and Metamaterials MURI (AFOSR Award FA9550-12-1-0488) and a Stanford Electrical Engineering Departmental Fellowship. S.R. is supported by a research grant (VKR023371) from VILLUM FONDEN. A.G.C. is supported by a Marie Curie International Outgoing Fellowship.

Author contributions

A.F.C. and M.L.B. conceived the idea. A.F.C., A.G.C. and M.L.B. designed the experiments. A.F.C. prepared the samples and carried out the experiments.

S.R. conducted the theoretical calculations. A.F.C. conducted full-field simulations. P.G.K. provided guidance during the simulations and experiments. All authors analysed and discussed the results and were involved in writing the manuscript.

Competing interests

The authors declare no competing interests.

Additional information

Supplementary information is available for this paper at https://doi.org/10.1038/s41566-018-0155-y.

Correspondence and requests for materials should be addressed to M.L.B.

Methods

Sample preparation and nanowire properties. The tapered nanowire discussed in Figs. 2–4 with the radius in the range of 20–40 nm, was grown in-house by a gold-catalysed chemical vapour deposition technique[4,60]. The second nanowire of this study, NW_2, with a radius of 88 nm, was purchased from Sigma-Aldrich. MoS_2 monolayer samples with semicontinuous areas, grown by chemical vapour deposition, were purchased from 2D Semiconductors. The granularity of photoluminescence maps in the paper is due to this imperfect surface coverage of MoS_2. The nanowires were drop casted on these MoS_2 samples from a colloidal suspension.

Note that while the drop-casting method does not give us specific control over the nanowire–emitter distance, it results in a very small variation in this separation thanks to the near-atomically flat MoS_2 layer and the single crystallinity of the Si nanowires. Therefore, the expected distance variation between the nanowire surface and the emitter layer is a few nanometres, small enough that the T/B ratio is not affected by it.

MoS_2 layer etching process. To eliminate the collection of emission from the MoS_2 areas that are not optically coupled to the nanowires, we exposed the sample to a mild Ar plasma etching process for 10 s in a sputtering system (AJA International). The nanowires themselves serve as a shadow mask protecting the emitter layer underneath while the rest of the MoS_2 monolayer is removed. Note that this etching procedure resulting in the narrowing of the MoS_2 region is not expected to modify the photoluminescence behaviour of the MoS_2 (no additional degradation is expected within the region masked by the nanowire, and the width of the MoS_2 is still too large for any quantum confinement effect to take place).

Photoluminescence imaging and spectroscopy. Experiments were conducted on a modified confocal microscope with top and bottom detection capabilities (WITec alpha300). The sample was excited with 633 nm continuous-wave laser through the top objective. The top detection path consists of an objective (Zeiss 100×, numerical aperture: 0.95), a linear polarizer, a laser filter (long pass with 650 nm cutoff), a fibre with a 20 μm core diameter serving as the confocal pinhole and a fibre-coupled avalanche photodiode (Micro Photon Devices). The bottom detection path consists of an objective (Zeiss 50×, numerical aperture: 0.55), a linear polarizer, a laser filter (long pass with 650 nm cutoff) and a free-space-coupled avalanche photodiode (Micro Photon Devices). The top objective was chosen to have a high numerical aperture to increase the excitation resolution of the system. The bottom objective, in contrast, was a long-working-distance objective to allow imaging through the transparent substrate and hence had a lower numerical aperture. The T/B ratio is calculated after a background subtraction from the top and bottom images.

One might notice the additional sharp peaks on the photoluminescence spectra in Fig. 4c. These additional peaks are expected to originate from the Raman scattering signals of the Si (at 655 nm and 675 nm), environment and localized contaminants.

FDTD simulations for reference and normalization procedure for T/B ratio analysis. Because of the inherent asymmetry of the top–bottom detection system (different objectives, free-space- versus fibre-coupled detection, beam splitter in the top direction for laser coupling, and the sample asymmetry due to substrate), a reference sample is needed to obtain a meaningful value for the T/B ratio. We used the T/B ratio of bare MoS_2 emission on sapphire substrate as a relevant reference. For this simple geometry, the T/B ratio is easily determined by 3D FDTD simulations, and this technique conveniently allows us to take into consideration the substrate effects. We calculate the T/B ratio of dipole emission from MoS_2 on sapphire substrate to be 0.8 in the wavelength range of interest (FDTD Solutions, Lumerical). The top and bottom emitted power values were obtained via power monitors with sizes corresponding to the numerical apertures of the experimental setup (top numerical aperture: 0.95, bottom numerical aperture: 0.55). Then, we normalized our experimental T/B ratio map such that the bare MoS_2 emission T/B ratio matches this value. Therefore, the resulting T/B ratio of more than 20 on the nanowire takes into consideration the asymmetry of the system and is purely thanks to the antenna's directionality enhancement. Hence, it can be concluded that 25 times the T/B ratio is the figure of merit of directionality for the antenna performance.

Modified Mie theory analysis of T/B ratio. T/B ratio values reported in Fig. 3a are obtained as

$$T/B = \int_{\theta=108.2^\circ}^{\theta=251.8^\circ} I_{\mathrm{ff}}(\theta)\,\mathrm{d}\theta \Big/ \int_{\theta=326.5^\circ}^{\theta=33.5^\circ} I_{\mathrm{ff}}(\theta)\,\mathrm{d}\theta \tag{3}$$

The integration limits were determined such that the calculated values correspond to the experiments with the correct numerical apertures: top = 0.95 and bottom = 0.55. Note that this calculation is for the emitter–antenna system in free space without a substrate. To confirm that the presence of the substrate is insignificant, we obtained the same parameter sweep result of the T/B ratio from FDTD simulations with a sapphire substrate (see Supplementary Fig. 6a). The comparison between the FDTD result involving the substrate (Supplementary Fig. 6a) and the analytical result (Fig. 3a) shows that the presence of the substrate is indeed not critical for the directionality in this system.

The significantly higher T/B ratios in calculations (and simulations in Supplementary Information) as compared with experiments are expected, as the calculations consider the emission from only one source dipole placed directly underneath the nanowire at an optimized spacing. In experiments, however, there will be a distribution of emitters from the MoS_2 region underneath the nanowire, which result in a deviation of the emitter-to-nanowire distance from the optimum. To check the validity of this explanation, we conducted simulations for the case with a distribution of dipoles under the nanowire and reported the results in Supplementary Fig. 7.

To further verify the validity of the 2D model and the simulations reported in the Supplementary Information, we also conducted a few exemplary 3D simulations showing the accuracy of the 2D modelling of the considered nanowire–emitter system (see Supplementary Fig. 4).

Finally, to investigate the potential effects of the asymmetric top–bottom detection paths with different numerical apertures, we ran a set of control simulations for the same sample but with identical top–bottom collection numerical apertures of 0.95. The results provided in Supplementary Fig. 6b show that, while the symmetric numerical apertures decrease the T/B ratio peak values, there is no noticeable change in the spectral behaviour of the peaks. This indicates that the directionality mechanism conclusions we obtained from the experiments remain valid.

Data availability. The data that support the plots within this paper and other findings of this study are available from the corresponding author upon reasonable request.

References

60. Cui, Y., Lauhon, L. J., Gudiksen, M. S., Wang, J. & Lieber, C. M. Diameter-controlled synthesis of single-crystal silicon nanowires. *Appl. Phys. Lett.* **78**, 2214–2216 (2001).